Heliyon 10 (2024) e24639

Contents lists available at ScienceDirect

Heliyon

journal homepage: www.cell.com/heliyon

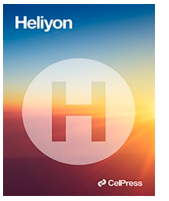

Research article

A new tannin-based adsorbent synthesized for rapid and selective recovery of palladium and gold: Optimization using central composite design

Farideh Zandi-Darehgharibi [a], Hedayat Haddadi [a,*], Arash Asfaram [b]

[a] Department of Chemistry, Faculty of Basic Sciences, Shahrekord University, Shahrekord, Iran
[b] Medicinal Plants Research Center, Yasuj University of Medical Sciences, Yasuj, Iran

ARTICLE INFO

Keywords:
Palladium
Gold
Selective recovery
Pomegranate peel tannin
Ethylenediamine
Electronic waste

ABSTRACT

A tannin-based adsorbent was synthesized by pomegranate peel tannin powder modified with ethylenediamine (PT-ED) for the rapid and selective recovery of palladium and gold. To characterize PT-ED, field emission scanning electron microscopy (FE-SEM), energy-dispersive X-ray spectroscopy (EDS-Mapping), and Fourier transform infrared spectroscopy (FT-IR) were used. Central composite design (CCD) was used for optimization. The kinetic, isotherm, interference of coexisting metal ions, and thermodynamics were studied. The optimal conditions, including Au (III) concentration = 30 $mg\,L^{-1}$, Pd (II) concentration = 30 $mg\,L^{-1}$, adsorbent mass = 26 mg, pH = 2, and time = 26 min with the sorption percent more than 99 %, were anticipated for both metals using CCD. Freundlich model and pseudo-second-order expressed the isotherm and kinetic adsorption of the both metals. The inhomogeneity of the adsorbent surface and the multi-layer adsorption of gold and palladium ions on the PT-ED surface are depicted by the Freundlich model. The thermodynamic investigation showed that Pd^{2+} and Au^{3+} ions adsorption via PT-ED was an endothermic, spontaneous, and feasible process. The maximum adsorption capacity of Pd^{2+} and Au^{3+} ions on PT-ED was 261.189 $mg\,g^{-1}$ and 220.277 $mg\,g^{-1}$, respectively. The probable adsorption mechanism of Pd^{2+} and Au^{3+} ions can be ion exchange and chelation. PT-ED (26 mg) recovered gold and palladium rapidly from the co-existing metals in the printed circuit board (PCB) scrap, including Ca, Zn, Si, Cr, Pb, Ni, Cu, Ba, W, Co, Mn, and Mg with supreme selectivity toward gold and palladium. The results of this work suggest the use of PT-ED with high selectivity and efficiency to recover palladium and gold from secondary sources such as PCB scrap.

1. Introduction

Precious metals are widely used in various areas such as the electronic industry, production of catalysts, production of corrosion-resistant materials, and production of jewelry, due to their special physicochemical properties, including high conductivity and corrosion resistance [1–3]. Today inexpensive technology constantly replaces old technology, creating a huge waste stream of obsolete electronic equipment. Electronic waste (e-waste) contains large amounts of precious metals such as Au and Pd, as well as base metals such as Cu, Zn, Ni, and Pb. Therefore, each ton of PCB on average includes 0.35 kg gold, 0.21 kg palladium, and 130 kg copper, which

* Corresponding author.
E-mail address: hedayathaddadi@Yahoo.com (H. Haddadi).

https://doi.org/10.1016/j.heliyon.2024.e24639
Received 26 August 2023; Received in revised form 8 December 2023; Accepted 11 January 2024
Available online 17 January 2024

gold and palladium have a significant economic value. For this reason, e-waste may be considered a secondary ore of precious metals [4–7]. Thus, the recovery of palladium and gold from e-waste is of significant economic and environmental importance. These metals can be effectively recycled from various wastes to be reused as they have finite resources that exist just in a small mass on the surface.

The recovery method should selectively isolate the precious metals from the base metals such as zinc and copper, which usually exist in excess amounts compared to the precious metals. Therefore, the development of efficient methods for the recovery of precious metals such as gold and palladium from a wide diversity of secondary sources is required. There are various methods such as hydrometallurgical, pyrometallurgical, solvent extraction, electrochemical extraction, adsorption with bio-sorbents, ion exchange resins, etc., to recover precious metals. Meanwhile, the adsorption technique with natural adsorbents is low cost, more straightforward, and more efficient [1–3,8].

According to the theory of hard and soft acids and bases, chelating agents, including N and S atoms, have a higher affinity to and greater selectivity for soft ions of metals such as Pd Cl_4^{2-}. Some ligands such as 2-aminothiazole, N-aminoguanidine, Plant tannin, Bisthiourea, Dimethylamine, and Ethylenediamine have been used to modify phenolic compounds and tannins to adsorb metal ions from e-waste. These ligands increase the adsorption capacity and allow the precious metals to be selectively recovered from base metals by forming complexes with them [6,9–14].

Parameters such as the concentration of the adsorbed components, time, amount of adsorbent, and pH have been proven to affect the efficiency of the adsorbent. Unlike the conventional methods of investigating a process, the experimental design technique is a more efficient, faster and more economical method that simultaneously optimizes the influential factors and possible interactions between them. One type of multivariate-based methods is Central Composite Design (CCD) under Response Surface Methodology (RSM), which provides a more reasonable prediction of the outcome response in fewer tests with minimal error [15–25].

This study was designed to rapidly and selectively recover gold and at the same time palladium from PCB scrap. For this purpose, tannin powder from pomegranate peel was modified with ethylenediamine ligand and effective parameters were optimized in the adsorption process via RSM-CCD.

2. Materials and method

2.1. Materials

Tannin-rich pomegranate peel was brought from Izeh County, Iran. Ethylenediamine, thiourea, formaldehyde, paraformaldehyde, NaOH, $HAuCl_4.xH_2O$, HNO_3, HCl, and $PdCl_2$ were bought from Merck Company. PCB scrap was obtained from a storage unit in Shahrekord University.

2.2. Synthesis and modification of the adsorbent

The tannin-rich pomegranate peel powder (28 g) was dissolved in 50 mL of NaOH solution (0.25 M) at ambient temperature, and then 6 mL of 37 % formaldehyde was added to it. Next, the mixture was heated to 353 K. The product was filtered after 12 h and ground. It was then rinsed several times with deionized water. This product dried at 338 K for 24 h. To modify the product obtained in the previous stage with ethylenediamine, 5 g of it was poured into a flask with 2.5 g of paraformaldehyde, and 30 mL of HCl (37 %) was added and the mixture was heated at 353 K for 2 h. Then 8 mL of ethylenediamine was added and stirred for 12 h at 363 K. Finally, the resin was filtered and rinsed several times with deionized water and dried at 338 K. It was then crushed into fine particles [6]. The modified tannin-rich pomegranate peel powder with ethylenediamine was called PT-ED. To characterize the adsorbent FE-SEM-EDS-Mapping and FT-IR were performed.

2.3. Design of experiment

The optimization of effective parameters in the adsorption process was accomplished using Design Expert, version 13, software. RSM-CCD was utilized to define the optimal value of each parameter at five levels of $-\alpha$ (−2), low (−1), center (0), high (+1), and $+\alpha$ (+2) There were ranges of factors, including Pd^{2+} and Au^{3+} ions concentration (20-60 $mg\,L^{-1}$), adsorbent mass (5–33 mg), contact time (5–33 min), and solution pH (1–5), and 26 tests were obtained in one block and a small mode. Table S1 displays the CCD experimental design parameters for metals adsorption by the PT-ED. Isotherm, kinetic, thermodynamic, and the effect of competing metals was evaluated using the optimal amounts acquired by CCD.

2.4. Experiments of the adsorption

Adsorption experiments designed by CCD were carried out to determine the effective factors. The thermostatic shaker at 200 rpm was used to shake the solutions. After the mixture was filtered, the resulting solution was used for an inductively coupled plasma mass spectrometry (ICP-MS) test. The adsorption percent of Pd^{2+} and Au^{3+} ions by PT-ED was computed using the following equation (1).

$$\%\,A = \frac{C_i - C_t}{C_i} \times 100 \tag{1}$$

Where C_i is the initial concentration of metals and C_t is the equilibrium concentration of metals in $mg\,L^{-1}$.

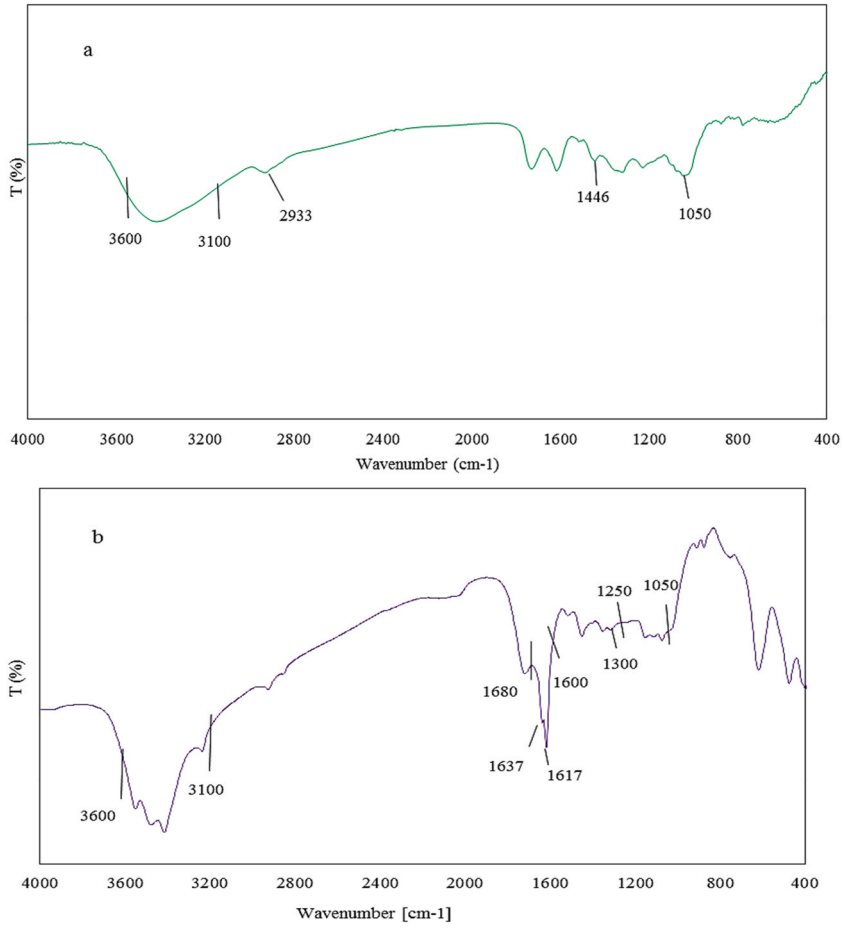

Fig. 1. FT-IR spectra of (a) tannin-rich pomegranate peel powder and (b) PT-ED.

After performing 26 tests designed by CCD, the optimal value of the influential parameters was determined, and using them, isotherm, kinetic, thermodynamic, and competition of metals tests were conducted according to the above conditions.

2.5. Acid digestion of the real sample

The plastic and other non-metallic materials of the PCB scrap were burned by the furnace at a temperature higher than 1023 K for 4 h. A planetary mill was then used to grind metals into fine particles. Reverse aqua regia (56 mL) was operated for the digestion of metal's fine particles (5 g) (37%w HCl (14 mL) and 69%w HNO_3 (42 mL)). Then it was heated for 2 h at 473 K. In the subsequent step, the cooled mixture was filtered, and finally, the concentration of metals in the solution (pH = 2) was defined via ICP-MS [26].

3. Results and discussion

3.1. Characterization of PT-ED

Fig. 1 shows the FT-IR spectra of (a) tannin-rich pomegranate peel powder and (b) PT-ED. The wide peaks at 3600-3100 cm^{-1} show the stretching vibration of the O—H group of phenolic [27–32]. The C—C bond of the ring was displayed at the wavelength 1446 cm^{-1} [12]. The small peak at 2933 cm^{-1} correspond to the C—H stretching of phenolic rings [31]. The C—O stretching vibration was displayed at 1050 cm^{-1} [33]. The peaks that emerged around 1640 and 1300 cm^{-1} are correlated with N–H bending and C–N stretching, respectively. The peak occurred at the wavelength of 1617 cm^{-1} indicates N–H bending. The changes observed in 1680-1600 cm^{-1} and 1250-1050 cm^{-1} regions of the spectrum (b) indicate the modification of the tannin-rich pomegranate peel powder with ethylenediamine [10,11].

Fig. 2 illustrates the results of the FE-SEM analysis. This experiment was conducted to study the PT-ED surface morphology. The pictures at varied magnifications showed that the PT-ED has a harsh, non-uniform, and spongy surface. Such a surface may cause palladium and gold ions to be adsorbed (Fig. 2 (a, b, and c)). The difference in the images of PT-ED after adsorption indicated that the

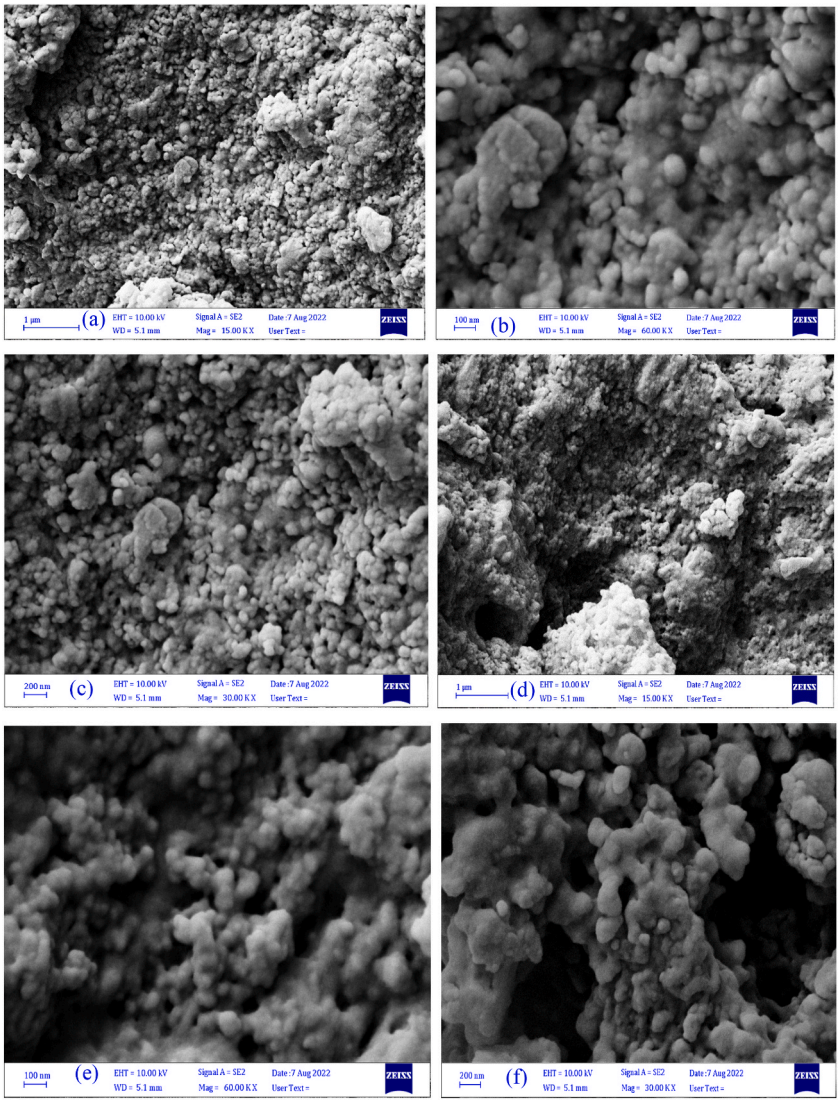

Fig. 2. FE-SEM of PT-ED (a, b, c) before adsorption and (d, e, f) after adsorption.

non-uniform surface of PT-ED was covered with the Pd^{2+} and Au^{3+} ions (Fig. 2 (d, e, and f)). In addition, EDS-mapping affirmed the adsorption of Pd and Au by the surface of PT-ED (Fig. 3 (c) and (d)).

The results of the EDS-mapping before and after the adsorption of Pd^{2+} and Au^{3+} ions on the PT-ED are shown in Fig. 3. Fig. 3 (a) shows EDS elemental analysis of the presence and weight percentage of C (66.3 %), O (24.2 %), and N (9.4 %) in the PT-ED before adsorption and Fig. 3 (c) shows EDS elemental analysis of the presence and weight percentage of C (67.2 %), O (21.3 %), N (9.3 %), Au (1.2 %) and Pd (1.0 %) after adsorption by PT-ED. Mapping analysis demonstrated how the elements were scattered in a specific area of the PT-ED surface (Fig. 3 (b) and (d)). EDS-mapping verified the sorption of palladium and gold by PT-ED surface.

3.2. Optimization condition of the adsorption

Acquiring the highest influence of diverse independent factors and their accompanying interaction on a process is called optimization [25]. Optimization was performed to attain the maximum adsorption conditions of Pd^{2+} and Au^{3+} ions on PT-ED by CCD and to determine the optimal value of the factors. Table S2 shows the CCD results. Under the conditions of Au (III) concentration = 30 $mg\,L^{-1}$, adsorbent mass = 26 mg, pH = 2, contact time = 26 min, and Pd (II) concentration = 30 $mg\,L^{-1}$, the adsorption percent for both metals with the desirability of 1.0 was expected to be greater than 99 %. The optimal conditions given by CCD were tested with three replicates, indicating a reasonable agreement between the obtained adsorption value (palladium adsorption of 99 %, and gold adsorption of 97 %) and the value expected from CCD.

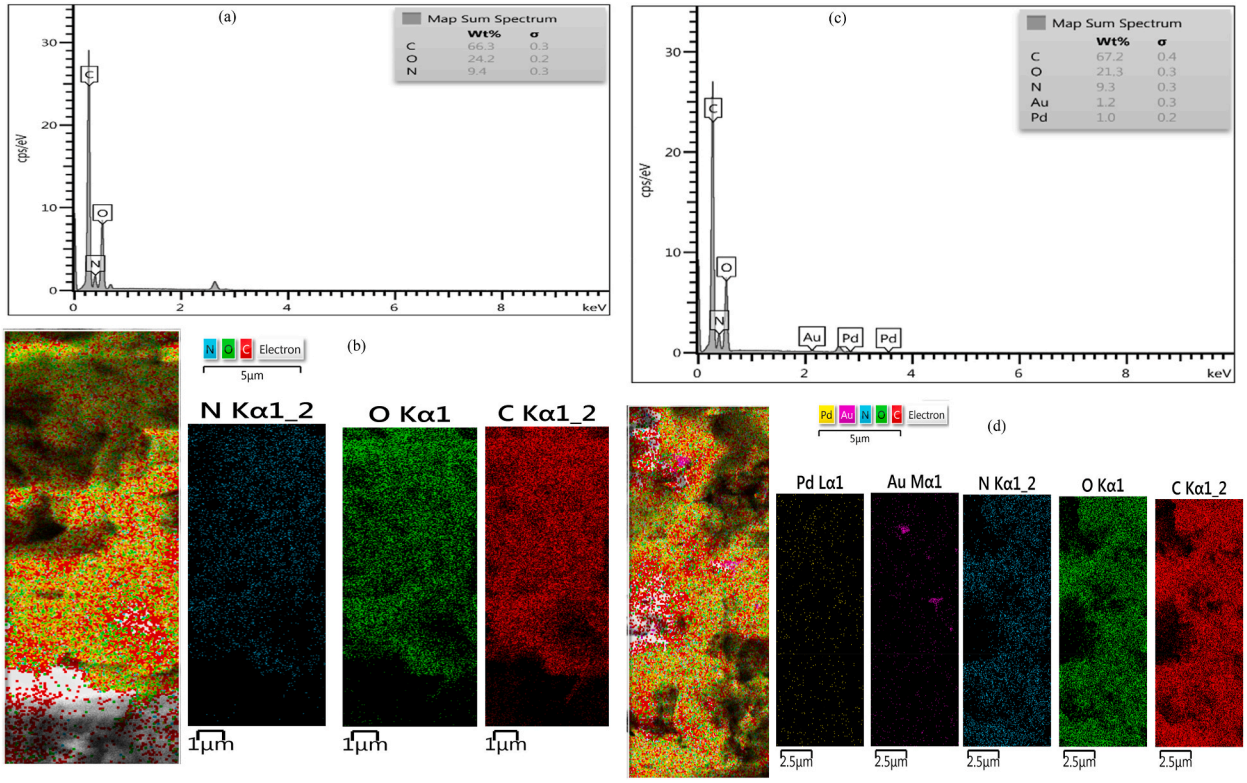

Fig. 3. EDS-Mapping of PT-ED (a) and (b) before adsorption and (c) and (d) after adsorption.

3.3. Analysis of variance (ANOVA)

The results of ANOVA and statistical summary of the model for the adsorption of Au^{3+} and Pd^{2+} ions by PT-ED are shown in Tables S3 and S4. The significance of the model for gold and palladium is shown by F = 2294.84 and F = 6436.03, respectively. For gold adsorption, the terms A, B, C, D, E, AB, AC, AD, AE, BC, CE, DE, A^2, B^2, C^2, and D^2 of the model are significant at $P < 0.05$. The significant terms of the model in palladium adsorption are A, B, C, D, E, AB, AC, AE, BC, BD, BE, CD, CE, DE, A^2, B^2, C^2, and E^2 at $P < 0.05$. The non-significance of the lack of fit of the models compared to the pure error was revealed by F = 0.46 for gold and F = 0.08 for palladium, and the non-significance of the lack of fit is satisfactory. The expected R^2 of 0.9936 and 0.9995 is in sensible agreement with the adjusted R^2 of 0.9995 and 0.9998 for gold and palladium, respectively. Adequate Precision is defined as the signal-to-noise ratio and a proportion larger than 4 is favorable. Adequate Precision for both metals was greater than 4.

3.4. Effect of factors interactions on palladium and gold adsorption percentage

The simultaneous influence of effective factors, including adsorbent mass, contact time, the concentration of palladium (II) and gold (III), and pH, on the adsorption of gold and palladium in the binary system of Pd^{2+} and Au^{3+} ions by PT-ED was examined. The three-dimensional plots (3D) of the gold and palladium adsorption via PT-ED are shown in Fi. 4.

3. 4. 1. Interaction between pH and the concentration of Pd^{2+} and Au^{3+} ions

As shown in Fig. 4 (a), the adsorption percentage of Pd^{2+} and Au^{3+} ions raised significantly with a concurrent decrease in the concentration of Au^{3+} and Pd^{2+} ions and pH. At a pH of about 2 and a concentration of about 40 $mg\ L^{-1}$, the adsorption percentage of Pd^{2+} and Au^{3+} ions reached 100 %. By increasing the concentration of Au^{3+} and Pd^{2+} ions, the number of functional groups of the PT-ED surface becomes less than the number of Au^{3+} and Pd^{2+} ions [34–36]. As a result, the active functional groups on the PT-ED surface are occupied very fast, and more functional groups are needed to adsorb the desired concentration. Hence, with an increase in the concentration of Pd^{2+} and Au^{3+} ions, adsorption was decreased.

3. 4. 2. Interaction of pH with the amount of adsorbent

The percentage of adsorption of Au^{3+} and Pd^{2+} ions was decreased by simultaneously raising pH levels and reduction of adsorbent mass (Fig. 4 (b)). The adsorption of metal anions through the PT-ED surface is dependent on the pH of the solution, which correspond the form of ionization of the PT-ED functional groups that affect the number of reachable active sites. Also, the pH of the solution

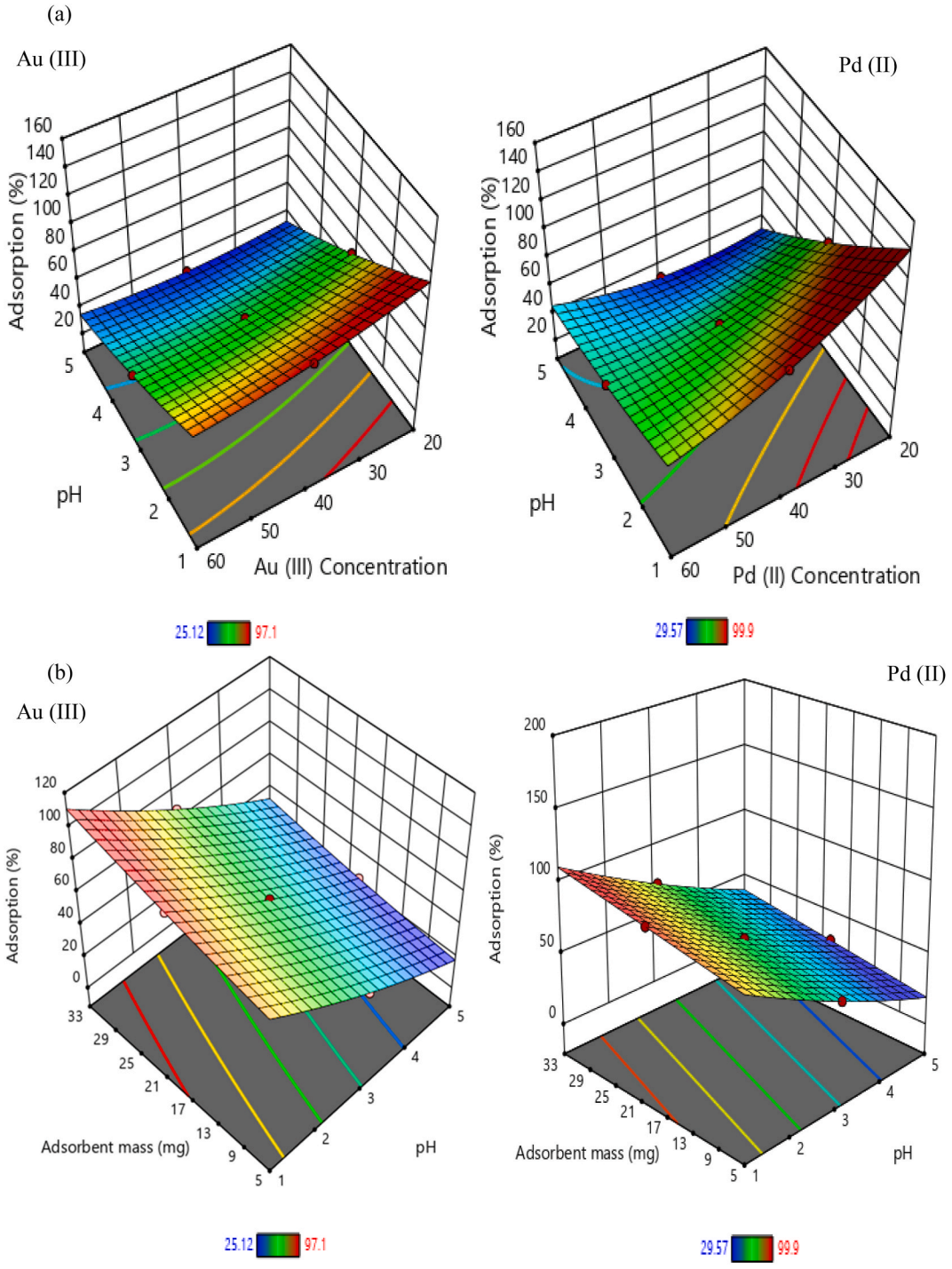

Fig. 4. 3D graphs of gold and palladium adsorption on PT-ED adsorbent. (a) interaction between pH and concentration of Au (III) and Pd (II) ions, (b) interaction between pH and amount of adsorbent, (c) interaction between pH and contact time, (d) interaction between the amount of adsorbent and concentration of Au (III) and Pd (II) ions, (e) interaction between the concentration of Au (III) and Pd (II) ions and contact time and (f) interaction between the amount of adsorbent and contact time. (For interpretation of the references to colour in this figure legend, the reader is referred to the Web version of this article.)

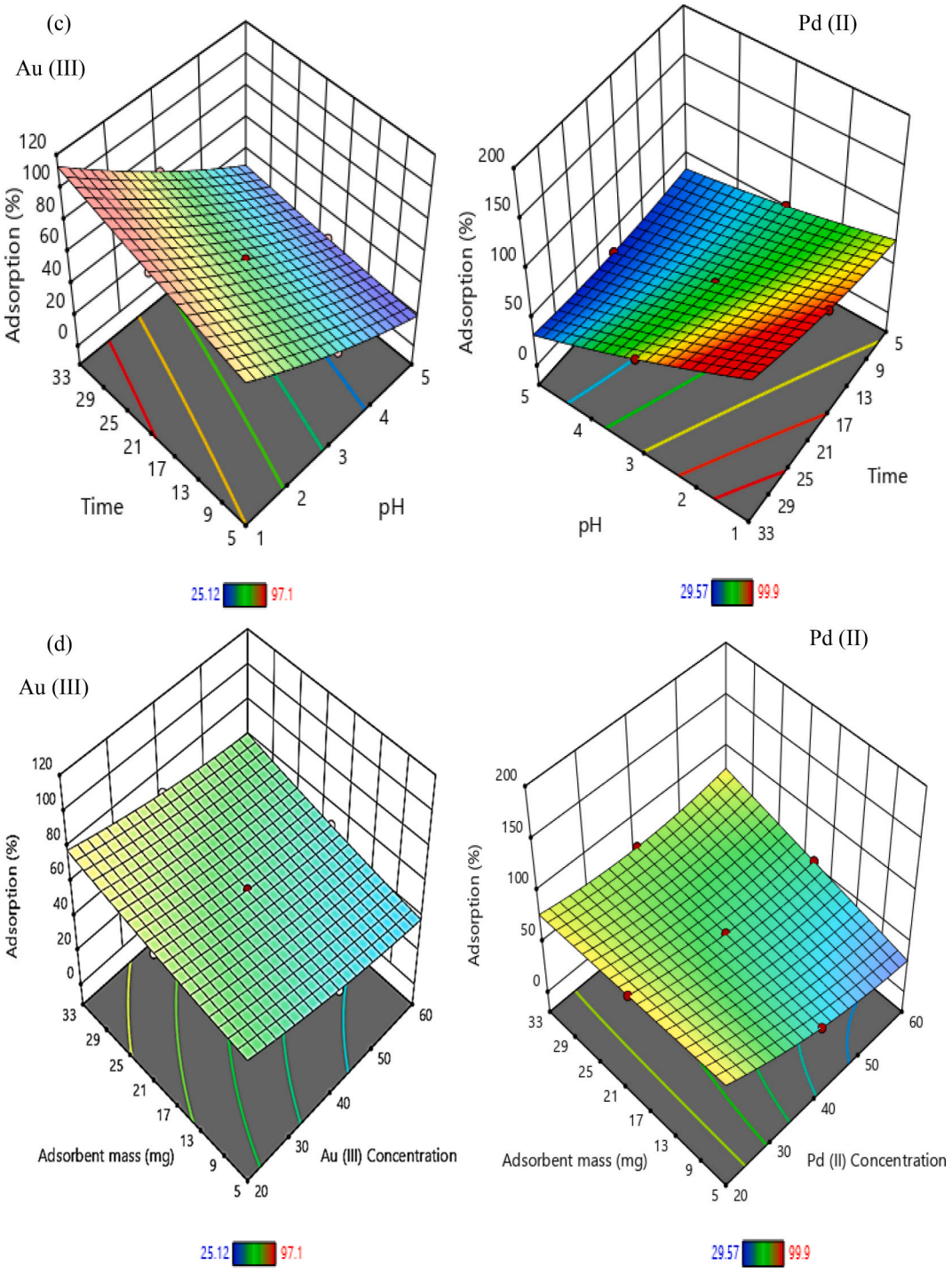

Fig. 4. (*continued*).

affects the ionization form of the metals in the solution [37,38].

The active sites of the PT-ED surface increase by increasing the PT- ED amount. Thus, the PT-ED could adsorb a large number of ions [34,39]. The pH less than 3 causes protonation (positive surface charge) of the PT-ED, and at this pH, the species of gold and palladium anions are Au Cl_4^- and Pd Cl_4^{2-} [29,40–45]. Therefore, Au Cl_4^- and Pd Cl_4^{2-} anions are absorbed by the positive charge of the PT-ED. Accordingly, these conditions are favorable for the adsorption of Au^{3+} and Pd^{2+} ions.

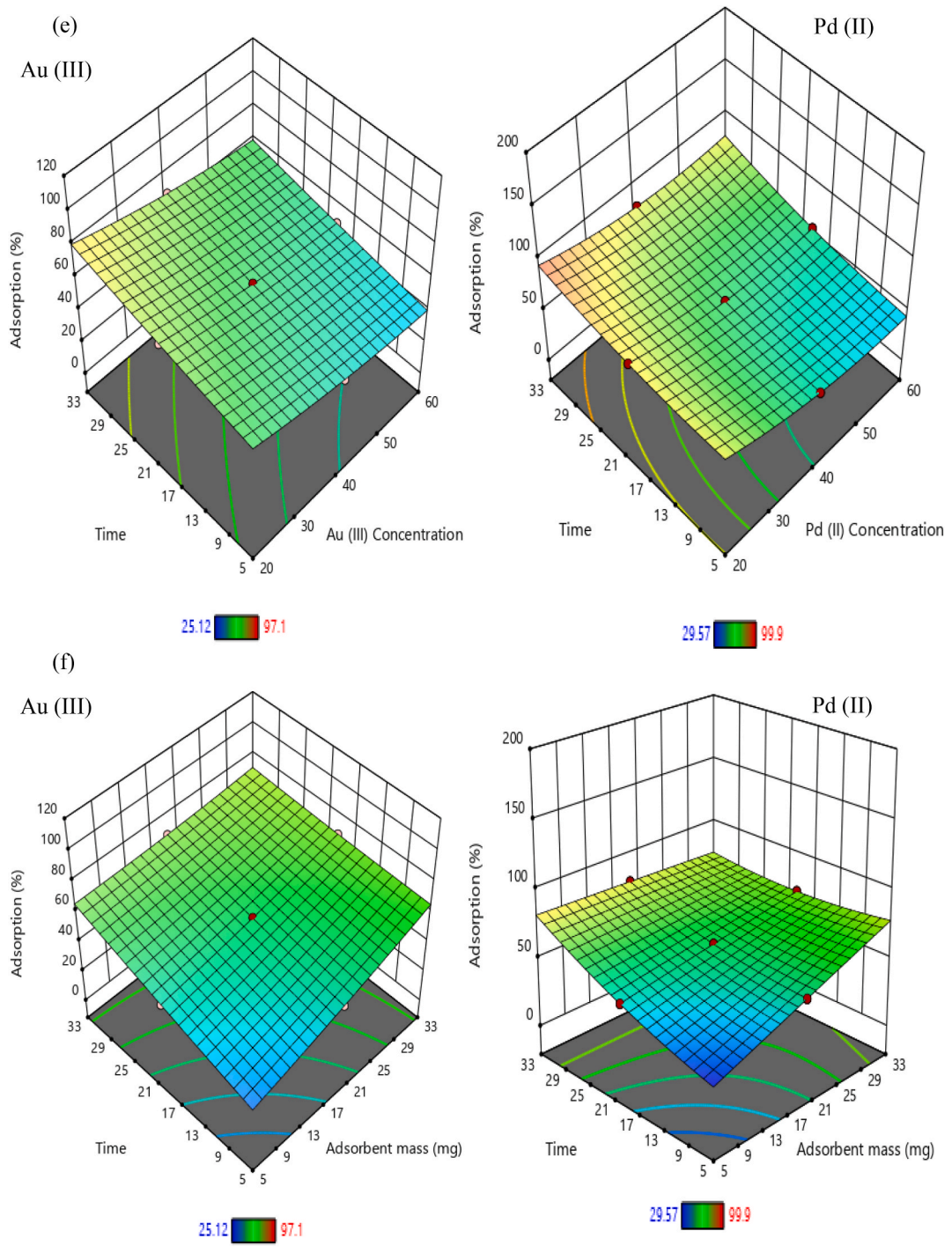

Fig. 4. (*continued*).

3. 4. 3. Interaction between time and pH

Fig. 4 (c) illustrates that with a simultaneous decrease in pH and a rise in time, the adsorption percentage of Au^{3+} and Pd^{2+} ions has increased significantly. In this situation, a decrease in pH causes the PT-ED surface charge to be positive and the Au Cl_4^- and Pd Cl_4^{2-} species to increase in the solution [42]. Also by increasing the contact time, the PT-ED found enough time to adsorb Au^{3+} and Pd^{2+} ions [19].

The possible rate of Au^{3+} and Pd^{2+} adsorption by the PT-ED is defined using the contact time. At pH equal to 1, about 20 min of time

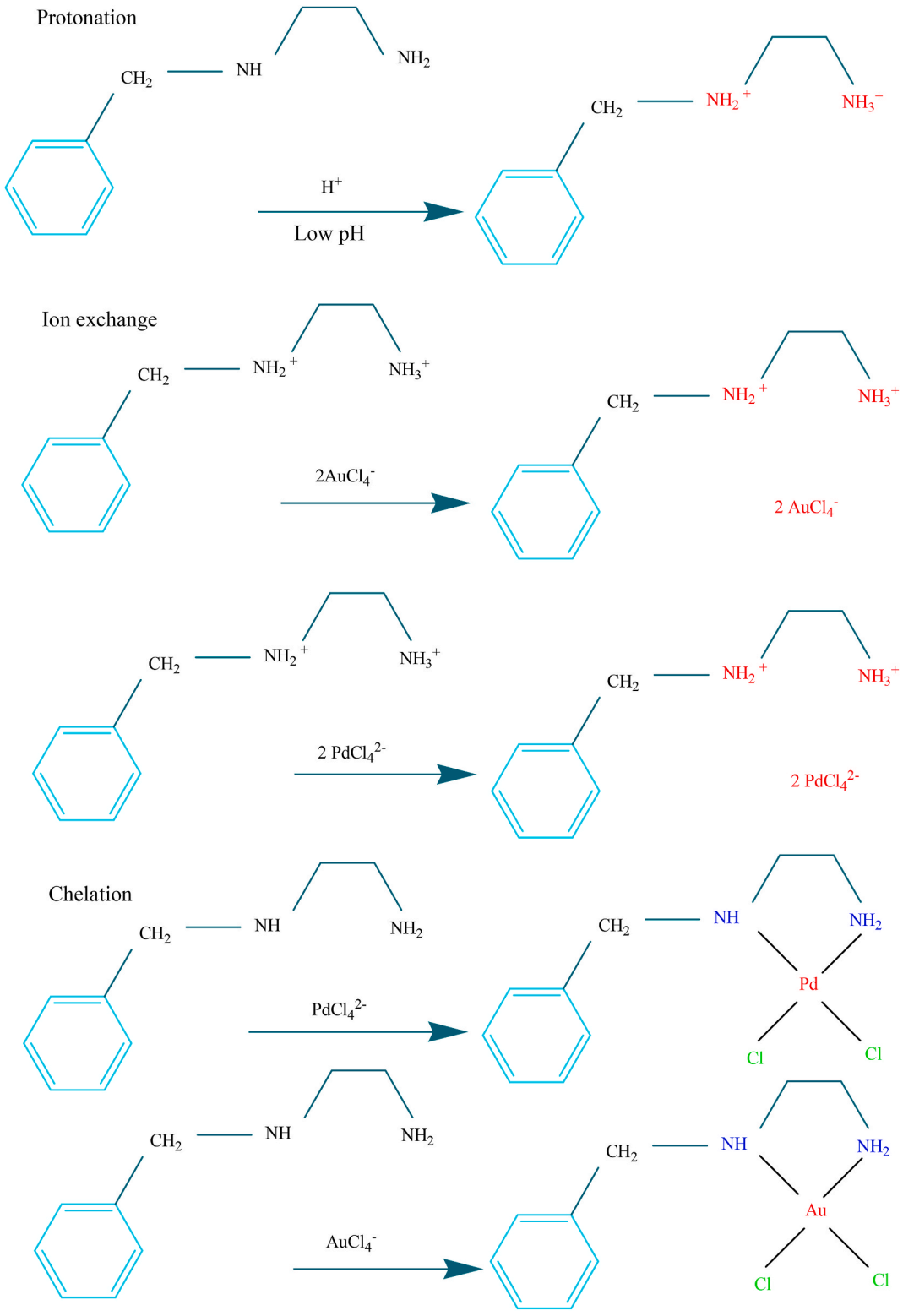

Fig. 5. Scheme of the probable mechanism of palladium and gold sorption by the PT-ED. (For interpretation of the references to colour in this figure legend, the reader is referred to the Web version of this article.)

is needed for the adsorption percentage to reach 100 %, indicating the rapid adsorption of Au^{3+} and Pd^{2+} ions on the PT-ED surface.

3. 4. 4. Interaction of the amount of adsorbent with Au^{3+} and Pd^{2+} ions concentration

As shown in Fig. 4 (d), with the simultaneous increase in the mass of the PT-ED and decrease in the concentration of Au^{3+} and Pd^{2+} ions, the adsorption percentage of palladium and gold was increased, which was significant for the adsorption of palladium ions. The number of active places on the PT-ED surface was raised with an increase in the amount of PT-ED. Moreover, the number of Pd^{2+} and Au^{3+} ions in the solution was diminished with a decrease in concentration [18,34,39,46]. Therefore, the large number of functional groups and the small number of ions in the solution cause an increase in the percent of Pd^{2+} and Au^{3+} ions adsorption by PT-ED. In addition, the significant adsorption percentage of palladium on the PT-ED surface indicates the remarkable affinity of PT-ED to adsorb Pd^{2+} ions.

3. 4. 5. Interaction between the concentration of Pd^{2+} and Au^{3+} ions and time

The interaction of Au^{3+} and Pd^{2+} ions concentration with time is shown in Fig. 4 (e). A redaction in the concentration and, simultaneously, an increase in the time cause the gold ions adsorption percent to rise and palladium ions sorption percent to increase significantly. Few ions in the solution and the increased time lead to an increase in the sorption [39,40]. These findings indicate that low concentration of Au^{3+} and Pd^{2+} ions and long-term shaking time increase the adsorption of Pd^{2+} and Au^{3+} ions on the PT-ED surface. In addition, the significant increase in the palladium adsorption percentage shows the high affinity of PT-ED to it.

3. 4. 6. Interaction between adsorbent mass and time

The interaction of adsorbent mass with time is displayed in Fig. 4 (f). With the simultaneous rise of PT-ED mass and contact time, the percentage of palladium ions adsorption was increased significantly and the percent of Au^{3+} sorption was raised. Increasing the amount of PT-ED causes an increase in the active functional groups on the surface of the PT-ED and increasing the contact time causes more metal ions to be adsorbed [19,39]. Thus, long-term shaking time and a large number of active places of the PT-ED lead to a rise in the amount of Pd^{2+} and Au^{3+} ions adsorption on the surface of the PT-ED. Furthermore, a significant increase in the palladium adsorption percentage signifies the excellent affinity of PT-ED to Pd^{2+} ions.

3.5. Mechanism of Au^{3+} and Pd^{2+} adsorption on PT-ED surface

The mechanism of adsorption of gold and palladium by adsorbents made with nitrogen-containing ligands in an acidic medium through ion exchange, electrostatic attraction, reduction, and chelation has been suggested in various studies [6,11,47].

Acidic conditions lead to the protonation of amine groups and the positive charge on the surface of the adsorbent containing them, while at pH less than 3, gold and palladium anions become chloro-complexes (Au Cl_4^- and Pd Cl_4^{2-}). Therefore, Au Cl_4^- and Pd Cl_4^{2-} anions are attracted to the PT-ED surface using electrostatic forces and anion exchange. Amine groups can form a 5-membered chelate complex with Pd Cl_4^{2-} anions and coordinate with Au Cl_4^- [6,11]. As a result, it is possible that nitrogen atoms in acidic pH with Pd Cl_4^{2-} and Au Cl_4^- anions lead to the formation of the 5-membered chelate complexes.

Consequently, the mechanism of palladium and gold adsorption by PT-ED may be ion exchange and chelation. A scheme of the probable mechanism of palladium and gold sorption by the PT-ED surface has been suggested in Fig. 5.

3.6. Isotherms models

Conventional isotherms of Dubinin-Radushkevich (D-R), Freundlich, Temkin, and Langmuir were used to examine the adsorption isotherm of gold and palladium on PT-ED [48–58]. The adsorbent capacity and the interaction between the adsorbent and the adsorbate are expressed by the adsorption isotherm. In the Langmuir model, the adsorbent surface is assumed to be homogeneous with adsorption sites having the same energy, and the adsorption of the adsorbed ingredient on the adsorbent surface is considered as a single layer [48–50]. The linear Langmuir equation (2) is as follows:

$$\frac{C_e}{q_e} = \frac{1}{Q_m k_L} + \frac{C_e}{Q_m} \tag{2}$$

Where C_e is the equilibrium concentration of the solute adsorbed ($mg\,L^{-1}$), q_e is the solute adsorbed amount per unit mass of the adsorbent ($mg\,g^{-1}$), Qm is the maximum capacity of the adsorbent ($mg\,g^{-1}$).

R_L is calculated by the following equation (3):

$$R_L = \frac{1}{1 + (k_L \times C_0)} \tag{3}$$

Where C_0 is the initial concentration of the adsorbed component ($mg\,L^{-1}$) and K_L is the Langmuir constant. The separation parameter R_L indicates the desirability of the adsorption process in such a way that $R_L = 0$ explains the irreversible adsorption process, $R_L > 1$ exhibits the disfavored adsorption process, $0 < R_L < 1$ confirms the eligible adsorption process, and $R_L = 1$ denotes linear adsorption process [48,49,58].

Table 1
Comparison of adsorption capacities of several adsorbents and time needed to reach equilibrium for Pd^{2+} and Au^{3+} ions adsorption.

Adsorbents	Adsorption capacity ($mg\,g^{-1}$)		pH		Time (h)		References
	Au (III)	Pd (II)	Au (III)	Pd (II)	Au (III)	Pd (II)	
DAVF-PT	535	214	2	3	24	24	[42]
GA	315.450	–	2	–	0.5	–	[58]
poly-Cys-g-PDA@GPUF	1082.6	784.5	1 M HCl	1 M HCl	0.5	0.5	[59]
GO	108.342	80.775	6	6	5	2.5	[60]
UiO-66-NH2	495	167	1	1	0.75	0.75	[61]
MPIDC	–	60.2	–	5.45	–	1.75	[62]
AC	–	35.70	–	2	–	1.67	[63]
BPMC	–	43.48	–	2	–	1.67	[63]
silica-based Thiol scavenger	–	105	–	1 M HNO_3	–	1	[64]
Zn–Al–LDH@ZIF–8	163	177	3.5	3.5	0.33	0.33	[65]
PPF resin	–	111.11	–	5	–	14	[66]
PT-ED	220.277	261.189	2	2	0.43	0.43	This work

The Freundlich model illustrates the adsorption process of the adsorbed molecules as multilayers on a heterogeneous adsorbent surface with various adsorption sites [48,49,54]. The linearized Freundlich equation (4) can be shown as follows:

$$log\ q_e = log\ K_F + \frac{1}{n} log\ C_e \tag{4}$$

The Freundlich constant is n, representing the surface inhomogeneity in the sorption system. The n value less than 1 ($n < 1$) points to the chemical adsorption process, n value of 1 ($n = 1$) represents the linear adsorption process, and the value greater than 1 ($n > 1$) implies the physical adsorption process [48,51,57]. K_F is the second Freundlich constant that depends on the adsorption capacity. A plot of log C_e versus log q_e provides a straight line, and the 1/n and K_F are calculated by the slope and the intercept of the line.

The state in which the heat of the adsorption dwindles linearly with the increase of adsorption capacity is defined by the Temkin model [48,49]. The Temkin equation (5) is presented below:

$$q_e = B_1\ ln\ K_T + B_1\ ln\ C_e \tag{5}$$

Tamkin's constants are B_1 ($J\,mol^{-1}$) and k_T ($L\,g^{-1}$), the former is related to the heat of the adsorption reaction, which is commensurate with the highest binding energy, and the latter is the equilibrium binding constant. A plot of qe versus ln Ce gives a straight line, and the values of B_1 and K_T could be acquired from the line's slope and intercept, respectively.

D-R expresses the mechanism of adsorption via the Gaussian distribution of energy on a heterogeneous surface [49,58]. The following equation (6) indicates the linear form of the D-R model:

$$ln\ q_e = \ln\ Q_s - \beta\varepsilon^2 \tag{6}$$

The plot of ln q_e versus ε^2 shows a straight line, and the values of β and ln Q_s could be acquired from the slope and intercept of the line.

The isotherm for both metals follows the Freundlich model with the value of R^2 being 0.956 and 0.938 for gold and palladium, respectively (Table S5). Therefore, the surface of the PT-ED is heterogeneous and both metals adsorption on the PT-ED surface is done in several layers. R_L was 0.062–0.284 for gold and 0.064–0.289 for palladium, indicating the favorable adsorption processes of the two metals. Table 1 shows the adsorption capacity of several adsorbents for gold and palladium. The highest adsorption capacity of PT-ED for Pd^{2+} and Au^{3+} was 261.189 $mg\,g^{-1}$ and 220.277 $mg\,g^{-1}$, respectively, indicating the PT-ED's good tendency to adsorb Au^{3+} ions and its excellent affinity to adsorb Pd^{2+} ions in comparison to other adsorbents.

3.7. Investigation of kinetic

To understand the interplay between the adsorbed component and the adsorbent, kinetic analyses were executed with the intra-particle diffusion, pseudo-first-order (PFO), Elovich, and pseudo-second-order (PSO) models [57,67–72]. When diffusion occurs in a monolayer where the change in the amount of sorption with time is proportional to the vacant places on the adsorbent surface, the model is PFO [49,68,72]. equation (7) of this model is shown below:

$$Log\ (q_e - q_t) = Log\ q_e - k_1 t \tag{7}$$

The rate constant of PFO is K_1 (min^{-1}), the mass of adsorbed at time t (min) is q_t, and the mass of adsorbed at saturation is q_e ($mg\,g^{-1}$).

The chemical interactions between the solute and the surface of the adsorbent are represented via the PSO model [49,68,72]. equation (8) of this model is as follows:

$$\frac{t}{q_t} = \frac{1}{k_2 + q_e^2} + \frac{t}{q_e} \tag{8}$$

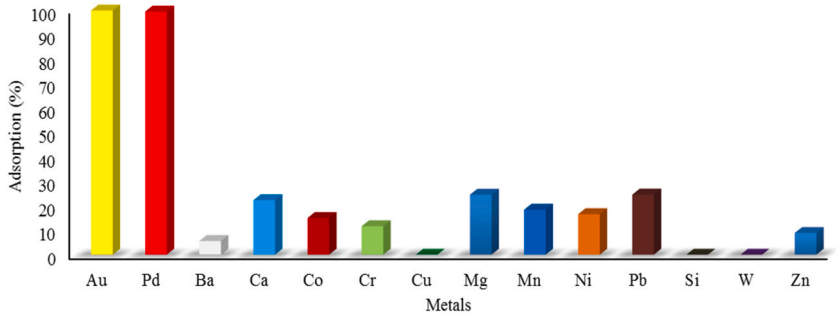

Fig. 6. Influence of co-existing metals in the PCB scarp on gold and palladium adsorption. (For interpretation of the references to colour in this figure legend, the reader is referred to the Web version of this article.)

Where K_2 (min^{-1}) is the rate constant of PSO and q_e ($mg\ g^{-1}$) is the amount of solute adsorbed in equilibrium.

Chemisorption is expressed via the Elovich model [48,49]. The equation of the Elovich model can be depicted using the following equation (9):

$$q_t = \frac{1}{\beta}\ln(t) + \frac{1}{\beta}\ln(\alpha\beta) \tag{9}$$

Which α ($mgg^{-1}\ min^{-1}$) indicates the initial speed of the adsorption reaction and β ($g\ mg^{-1}$) shows the range of the surface coverage and activation energy.

The speed control step and the steps affecting the speed of the sorption process are defined by the intra-particle diffusion [48,58, 69]. equation (10) of this model is as follows:

$$q_t = k_{diff} t^{1/2} + C \tag{10}$$

Where K_{diff} and C represent the intra-particle diffusion rate constant and boundary surface layer thickness, respectively.

The main parameters of kinetic models are demonstrated in Table S6. For both metals, the R^2 value of the PSO model was the nearest value to 1 ($R^2 = 0.999$) and it was greater than the R^2 value of the other models. Thus, the PSO model is suited to characterize the kinetic of Pd^{2+} and Au^{3+} adsorption processes on the PT-ED surface. In addition, the q_e values obtained and computed by the PSO model are very near to each other, indicating that this model is very fit for displaying the testing data. These findings reveal the interactions of Pd^{2+} and Au^{3+} ions with the PT-ED surface may be chemical. Table 1 shows the time needed to achieve PT-ED equilibrium in comparison to various adsorbents. The adsorption of gold and palladium onto PT-ED achieves equilibrium in a briefer time as compared to other adsorbents, showing the rapid adsorption of Pd^{2+} and Au^{3+} ions by PT-ED.

3.8. Thermodynamic investigation

The impact of temperature on Pd^{2+} and Au^{3+} ions adsorption at various temperatures was examined. The entropy (ΔS^0), enthalpy (ΔH^0), and Gibbs free energy (ΔG^0), as thermodynamic parameters, were calculated by the following equations 11–13 [73–78].

$$K_d = \frac{C_{ads}}{C_e} \tag{11}$$

$$\mathrm{Ln}\ K_d = -\frac{\Delta H^0}{RT} + \frac{\Delta S^0}{R} \tag{12}$$

$$\Delta G^0 = -\ \mathrm{RTLn}\ K_d \tag{13}$$

Where K_d is the distribution coefficient of adsorption, C_{ads} is the value of Pd^{2+} and Au^{3+} ions adsorbed via the PT-ED at equilibrium (mg L^{-1}), C_e is the quantity of Pd^{2+} and Au^{3+} ions remaining at equilibrium (mg L^{-1}), T (K°) is the temperature of the solution, and R (8.314 J $mol^{-1}\ K^{-1}$) is the universal gas constant. The quantity of ΔS^0 and ΔH^0 was measured from the slope and intercept of the Ln K_d plot against $\frac{1}{T}$.

As shown in Table S7, the percent of gold and palladium adsorption by PT-ED increased with an increase in temperature. An entropy value greater than zero ($\Delta S^0 > 0$) denotes an increase in disorder. Gibbs free energy less than zero ($\Delta G^0 < 0$) means that the process of adsorption is spontaneous. The endothermic process of gold and palladium adsorption by PT-ED is confirmed with an enthalpy greater than zero ($\Delta H^0 > 0$).

Table 2
Comparison of adsorbent mass and the number of co-existing metals of various adsorbents for gold and palladium adsorption.

Adsorbents	Metal	Adsorbent Mass (mg)	Competing Metals	References
DMA-PP gel	Au/Pd	10	Ni, Zn, Cu, Fe, Pt	[14]
PT-GO	Au/Pd	50	Ag	[36]
UiO-66-NH2	Au/Pd	10	Cu, Ni, Co, Zn	[61]
Mag-GO@MBT/SDS NPs	Au/Pd	30	Fe, Mn, Cu, Pb, Zn, Co, Mo, Ni, Cr, Cd	[79]
PT-ED	Au/Pd	26	Si, Zn, Pb, Ba, Ni, Ca, Co, Cr, Mn, Cu, Mg, W	This work

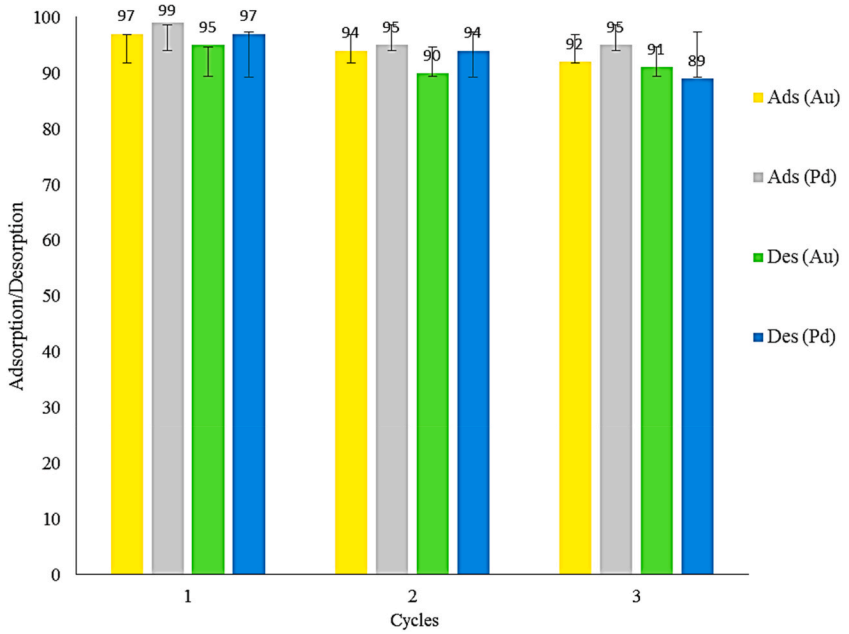

Fig. 7. Reusability of PT-ED.

3.9. *Influence of co-existing metals in the real sample on the gold and palladium adsorption*

Metals existent in the real sample matrix could influence the adsorption of palladium and gold by the PT-ED. Consequently, it is necessary to test the selectivity of the PT-ED to palladium and gold in the company of competing metals. The PT-ED evaluation for the recovery of gold and palladium in the matrix of waste PCB in the presence of competing metals with different concentrations was accomplished under optimal conditions, including adsorbent mass = 26 mg, pH = 2, and contact time = 26 min (Fig. 6). As is observed in Fig. 6, PT-ED has shown a very high selectivity for adsorbing gold and palladium compared to other metals, and its tendency to adsorb other metals was negligible and close to zero. Base metal ions exist in the acidic medium in cationic or neutral species, but palladium and gold ions exist in the anionic form in this medium [11,29,42,47]. Therefore, the PT-ED does not tend to adsorb base metal ions because of its positive surface charge.

Metal ions with ligands that have more or less electronegative donor atoms have a greater preference for complex formation. Chelating agents with nitrogen atoms are effective for the selective adsorption of precious metal ions. According to Pearson's theory, ethylenediamine tends to adsorb soft metals such as palladium and gold due to the existence of soft nitrogen atoms and does not tend to adsorb hard or medium metals. N donor atoms have a weak tendency to form complexes with base metals in less acidic solutions [79, 80].

Table 2 indicates the mass of adsorbent and co-existing metals of different adsorbents for the adsorption of gold and palladium. A small mass of PT-ED recovered gold and palladium from a larger number of co-existing metals existing in the PCB scrap compared to other adsorbents.

3.10. *Reusability of PT-ED*

The adsorption efficacy of the regenerated PT-ED was assessed in three consecutive cycles and experimental conditions, including Au (III) concentration = 30 $mg\,L^{-1}$, Pd (II) concentration = 30 $mg\,L^{-1}$, pH = 2, temperature = 303 K, adsorbent mass = 26 mg, and contact time = 26 min. The elution of precious metals adsorbed on the surface of PT-ED was done using thiourea in HCl (0.5 M: 2 M) and the shaking time was 4 h [58]. As shown in Fig. 7, the adsorption percent of the PT-ED is more than 90 % in three cycles for both

metals. These results represent the ability of PT-ED to be regenerated and reused; therefore, the use of PT-ED could be economical.

4. Conclusion

In this study, the powder of pomegranate peel tannins was modified with ethylenediamine ligand. The modified adsorbent was used for the rapid and selective recovery of Pd^{2+} and Au^{3+} ions from waste PCB. The optimal conditions, including Au (III) concentration = 30 $mg\,L^{-1}$, adsorbent mass = 26 mg, pH = 2, contact time = 26 min, and Pd (II) concentration = 30 $mg\,L^{-1}$ with the sorption percent more than 99 %, was anticipated with a 0.1 desirability using CCD for both metals. The sorption percent obtained with three replications under optimal conditions was 97 % for gold and 99 % for palladium, which was in good agreement with the expected values. The adsorption isotherm for both metals was determined by the Freundlich model ($R^2 = 0.956$) for gold and ($R^2 = 0.938$) for palladium. The PSO model ($R^2 = 0.999$) expressed the adsorption kinetic of Pd^{2+} and Au^{3+} ions on PT-ED. The thermodynamics of Pd^{2+} and Au^{3+} ions adsorption by the PT-ED was an endothermic ($\Delta H^\circ > 0$), straightforward ($\Delta S^\circ > 0$), and spontaneous ($\Delta G^\circ < 0$) process. The highest capacity of the PT-ED to adsorb Pd^{2+} and Au^{3+} ions was 261.189 $mg\,g^{-1}$ and 220.277 $mg\,g^{-1}$, respectively. A small mass of the PT-ED rapidly recovered gold and palladium from the competing metals in PCB scrap, including Ca, Zn, Si, Cr, Pb, Ni, Cu, Ba, W, Co, Mn, and Mg with excellent selectivity toward gold and palladium. The results of this research indicate the potency of PT-ED with high selectivity and efficiency in recovering gold and palladium from secondary sources such as PCB scrap.

Data availability statement

The data supporting the results of this study are contained within the paper and supplementary material.

CRediT authorship contribution statement

Farideh Zandi-Darehgharibi: Writing – review & editing, Writing – original draft, Software, Resources, Methodology, Investigation, Formal analysis, Data curation, Conceptualization. **Hedayat Haddadi:** Visualization, Validation, Supervision, Project administration, Resources. **Arash Asfaram:** Software, Resources, Methodology, Conceptualization.

Declaration of competing interest

The authors declare that they have no known competing financial interests or personal relationships that could have appeared to influence the work reported in this paper.

Acknowledgments

We thank everyone who helped us in this work. This work was supported by Shahrekord University.

Appendix A. Supplementary data

Supplementary data to this article can be found online at https://doi.org/10.1016/j.heliyon.2024.e24639.

References

[1] O. Buriac, M. Ciopec, N. Duţeanu, A. Negrea, P. Negrea, I. Grozav, Platinum (IV) recovery from waste solutions by adsorption onto dibenzo-30-crown-10 ether immobilized on Amberlite XAD7 resin–factorial design analysis, Molecules 25 (2020) 3692, https://doi.org/10.3390/molecules25163692.
[2] M. Mihăilescu, A. Negrea, M. Ciopec, C.M. Davidescu, P. Negrea, N. Duţeanu, G. Rusu, Gold (III) adsorption from dilute waste solutions onto Amberlite XAD7 resin modified with L-glutamic acid, Sci. Rep. 9 (2019) 8757, https://doi.org/10.1038/s41598-019-45249-1.
[3] C. Ianăşi, P. Svera, A. Popa, R. Lazău, A. Negrea, P. Negrea, N. Duteanu, M. Ciopec, N.S. Nemes, Adsorbent material based on carbon black and bismuth with tunable properties for gold recovery, Materials 16 (2023) 2837, https://doi.org/10.3390/ma16072837.
[4] H.Y. Kang, J.M. Schoenung, Electronic waste recycling: a review of U.S. infrastructure and technology options, Resour. Conserv. Recycl. 45 (2005) 368–400, https://doi.org/10.1016/j.resconrec.2005.06.001.
[5] T. Ogata, Y. Nakano, Mechanisms of gold recovery from aqueous solutions using a novel tannin gel adsorbent synthesized from natural condensed tannin, Water Res. 39 (2005) 4281–4286, https://doi.org/10.1016/j.watres.2005.06.036.
[6] Q. Yi, R. Fan, F. Xie, H. Min, Q. Zhang, Z. Luo, Selective recovery of Au(III) and Pd(II) from waste PCBs using ethylenediamine modified persimmon tannin adsorbent, Procedia Environ. Sci. 31 (2016) 185–194, https://doi.org/10.1016/j.proenv.2016.02.025.
[7] X. Zeng, J.A. Mathews, J. Li, Urban mining of E - waste is becoming more cost-E ff ective than virgin mining, Environ. Sci. Technol. 52 (2018) 4835–4841, https://doi.org/10.1021/acs.est.7b04909.
[8] M. Gurung, B.B. Adhikari, H. Kawakita, K. Ohto, K. Inoue, S. Alam, Recovery of Au(III) by using low cost adsorbent prepared from persimmon tannin extract, Chem. Eng. J. 174 (2011) 556–563, https://doi.org/10.1016/j.cej.2011.09.039.
[9] C.R. Adhikari, D. Parajuli, H. Kawakita, K. Inoue, K. Ohto, H. Harada, Dimethylamine-modified waste paper for the recovery of precious metals, Environ. Sci. Technol. 42 (2008) 5486–5491, https://doi.org/10.1021/es800155x.
[10] M. Gurung, B.B. Adhikari, H. Kawakita, K. Ohto, K. Inoue, Selective recovery of precious metals from acidic leach liquor of circuit boards of spent mobile phones using chemically modified persimmon tannin gel, Ind. Eng. Chem. Res. 51 (2012) 11901–11913, https://doi.org/10.1021/ie3009023.

[11] M. Gurung, B. Babu, S. Morisada, H. Kawakita, K. Ohto, N -aminoguanidine modified persimmon tannin : a new sustainable material for selective adsorption, preconcentration and recovery of precious metals from acidic chloride solution, Bioresour. Technol. 129 (2013) 108–117, https://doi.org/10.1016/j.biortech.2012.11.012.

[12] R. Fan, H. Min, X. Hong, Q. Yi, W. Liu, Q. Zhang, Z. Luo, Plant tannin immobilized Fe_3O_4@SiO_2 microspheres: a novel and green magnetic bio-sorbent with superior adsorption capacities for gold and palladium, J. Hazard Mater. 364 (2019) 780–790, https://doi.org/10.1016/j.jhazmat.2018.05.061.

[13] G. Lin, S. Wang, L. Zhang, T. Hu, J. Peng, Selective recovery of Au (III) from aqueous solutions using 2- aminothiazole functionalized corn bract as low-cost bioadsorbent, J. Clean. Prod. 196 (2018) 1007–1015, https://doi.org/10.1016/j.jclepro.2018.06.168.

[14] Y. Xiong, C.R. Adhikari, H. Kawakita, K. Ohto, H. Harada, K. Inoue, Recovery of precious metals by selective adsorption on dimethylamine- modified persimmon peel, Waste Biomass Valorization 1 (2010) 339–345, https://doi.org/10.1007/s12649-010-9029-3.

[15] A. Tadjarodi, S. Moazen Ferdowsi, R. Zare-Dorabei, A. Barzin, Highly efficient ultrasonic-assisted removal of Hg(II) ions on graphene oxide modified with 2-pyridinecarboxaldehyde thiosemicarbazone: adsorption isotherms and kinetics studies, Ultrason. Sonochem. 33 (2016) 118–128, https://doi.org/10.1016/j.ultsonch.2016.04.030.

[16] M.S. Tehrani, R. Zare-Dorabei, Competitive removal of hazardous dyes from aqueous solution by MIL-68(Al): derivative spectrophotometric method and response surface methodology approach, Spectrochim. Acta Mol. Biomol. Spectrosc. 160 (2016) 8–18, https://doi.org/10.1016/j.saa.2016.02.002.

[17] F. Nasiri Azad, M. Ghaedi, K. Dashtian, S. Hajati, A. Goudarzi, M. Jamshidi, Enhanced simultaneous removal of malachite green and safranin O by ZnO nanorod-loaded activated carbon: modeling, optimization and adsorption isotherms, New J. Chem. 39 (2015) 7998–8005, https://doi.org/10.1039/c5nj01281c.

[18] M. Sheydaei, A.B. Gasemsoltanlu, A. Beiraghi, Optimization of ultrasonic-assisted copper ion removal from polluted water by a natural clinoptilolite nanostructure through a central composite design, Clay Miner. 54 (2019) 339–347, https://doi.org/10.1180/clm.2019.46.

[19] P. Arabkhani, H. Javadian, A. Asfaram, S.N. Hosseini, A reusable mesoporous adsorbent for efficient treatment of hazardous triphenylmethane dye wastewater: RSM-CCD optimization and rapid microwave-assisted regeneration, Sci. Rep. 11 (2021) 1–18, https://doi.org/10.1038/s41598-021-02213-2.

[20] M. Foschi, P. Capasso, M.A. Maggi, F. Ruggieri, G. Fioravanti, Experimental design and response surface methodology applied to graphene oxide reduction for adsorption of triazine herbicides, ACS Omega 6 (2021) 16943–16954, https://doi.org/10.1021/acsomega.1c01877.

[21] A.R. Bagheri, M. Ghaedi, A. Asfaram, R. Jannesar, A. Goudarzi, Design and construction of nanoscale material for ultrasonic assisted adsorption of dyes: application of derivative spectrophotometry and experimental design methodology, Ultrason. Sonochem. 35 (2017) 112–123, https://doi.org/10.1016/j.ultsonch.2016.09.008.

[22] A.R. Bagheri, M. Ghaedi, A. Asfaram, A.A. Bazrafshan, R. Jannesar, Comparative study on ultrasonic assisted adsorption of dyes from single system onto Fe_3O_4 magnetite nanoparticles loaded on activated carbon: experimental design methodology, Ultrason. Sonochem. 34 (2017) 294–304, https://doi.org/10.1016/j.ultsonch.2016.05.047.

[23] E. Sharifpour, H. Haddadi, M. Ghaedi, K. Dashtian, A. Asfaram, Synthesis of antimicrobial cationic amphiphile functionalized mesocellular silica foam prepared on hard template/support activated carbon for enhanced simultaneous removal of Cu(II) and Zn(II) ions, J. Environ. Chem. Eng. 6 (2018) 4864–4877, https://doi.org/10.1016/j.jece.2018.07.029.

[24] E. Sharifpour, H. Haddadi, M. Ghaedi, A. Asfaram, S. Wang, Simultaneous and rapid dye removal in the presence of ultrasound waves and a nano structured material: experimental design methodology, equilibrium and kinetics, RSC Adv. 6 (2016) 66311–66319, https://doi.org/10.1039/c6ra13286c.

[25] R. Singh, R. Bhateria, Optimization and experimental design of the Pb^{2+}adsorption process on a nano-Fe3O4-based adsorbent using the response surface methodology, ACS Omega 5 (2020) 28305–28318, https://doi.org/10.1021/acsomega.0c04284.

[26] A. Hubau, A. Chagnes, M. Minier, S. Touzé, S. Chapron, A.G. Guezennec, Recycling-oriented methodology to sample and characterize the metal composition of waste Printed Circuit Boards, Waste Manage. (Tucson, Ariz.) 91 (2019) 62–71, https://doi.org/10.1016/j.wasman.2019.04.041.

[27] A. Asfaram, M. Ghaedi, M.H.A. Azqhandi, A. Goudarzi, M. Dastkhoon, Statistical experimental design, least squares-support vector machine (LS-SVM) and artificial neural network (ANN) methods for modeling the facilitated adsorption of methylene blue dye, RSC Adv. 6 (2016) 40502–40516, https://doi.org/10.1039/c6ra01874b.

[28] P.B. Raja, A.A. Rahim, A.K. Qureshi, K. Awang, Green synthesis of silver nanoparticles using tannins, Mater. Sci.-Pol. 32 (2014) 408–413, https://doi.org/10.2478/s13536-014-0204-2.

[29] F. Liu, L. Zhou, L. Tao, L. Qian, G. Yu, S. Deng, Adsorption behavior and mechanism of Au(III) on caffeic acid functionalized viscose staple fibers, Chemosphere 253 (2020) 126704, https://doi.org/10.1016/j.chemosphere.2020.126704.

[30] F. Xie, Z. Fan, Q. Zhang, Z. Luo, Selective adsorption of Au^{3+} from aqueous solutions using persimmon powder-formaldehyde resin, J. Appl. Polym. Sci. 130 (2013) 3937–3946, https://doi.org/10.1002/app.39521.

[31] F.G. Mendonça, T.G. Silva, G.M. do Nascimento, H.O. Stumpf, R.V. Mambrini, W.D. do Pim, Human hair as adsorbent of palladium(II) in solution: a precursor of well-dispersed size-controlled Pd nanoparticles, J. Braz. Chem. Soc. 30 (2019) 736–743, https://doi.org/10.21577/0103-5053.20180194.

[32] L. Abed, N. Belattar, Polyphenols content, chelating properties and adsorption isotherms and kinetics of red and yellow pomegranate peels (punica granatum L.) towards lead (II), Pol. J. Environ. Stud. 31 (2022) 5765–5779, https://doi.org/10.15244/pjoes/152381.

[33] Y. Boutaleb, R. Zerdoum, N. Bensid, R.A. Abumousa, Z. Hattab, M. Bououdina, Adsorption of Cr (VI) by mesoporous pomegranate peel biowaste from synthetic wastewater under dynamic mode, Water 23 (2022) 3885, https://doi.org/10.3390/w14233885.

[34] P. Arabkhani, A. Asfaram, Development of a novel three-dimensional magnetic polymer aerogel as an efficient adsorbent for malachite green removal, J. Hazard Mater. 384 (2020) 121394, https://doi.org/10.1016/j.jhazmat.2019.121394.

[35] S.Y. Hashemi, M.Y. Badi, H. Pasalari, A. Azari, H. Arfaeinia, A. Kiani, Degradation of Ceftriaxone from aquatic solution using a heterogeneous and reusable O_3/UV/Fe_3O_4@TiO_2 systems : operational factors , kinetics and mineralisation, J. Environ. Anal. Chem. 00 (2020) 1–17, https://doi.org/10.1080/03067319.2020.1817909.

[36] Z. Wang, X. Li, H. Liang, J. Ning, Z. Zhou, G. Li, Equilibrium, kinetics and mechanism of Au^{3+}, Pd^{2+} and Ag^{+} ions adsorption from aqueous solutions by graphene oxide functionalized persimmon tannin, Mater. Sci. Eng. C. 79 (2017) 227–236, https://doi.org/10.1016/j.msec.2017.05.038.

[37] H.I. Adegoke, F. AmooAdekola, O.S. Fatoki, B.J. Ximba, Adsorption of Cr (VI) on synthetic hematite (α-Fe_2O_3) nanoparticles of different morphologies, Korean J. Chem. Eng. 31 (2014) 142–154, https://doi.org/10.1007/s11814-013-0204-7.

[38] A.F. Ngomsik, A. Bee, J.M. Siaugue, D. Talbot, V. Cabuil, G. Cote, Co(II) removal by magnetic alginate beads containing Cyanex 272 ®, J. Hazard Mater. 166 (2009) 1043–1049, https://doi.org/10.1016/j.jhazmat.2008.11.109.

[39] R. Panda, O.S. Dinkar, M.K. Jha, D.D. Pathak, Novel approach for selective recovery of gold, copper, and iron as marketable product from industrial effluent, Gold Bull. 53 (2020) 11–18, https://doi.org/10.1007/s13404-020-00269-y.

[40] L. Tofan, I. Bunia, C. Paduraru, C. Teodosiu, Synthesis, characterization and experimental assessment of a novel functionalized macroporous acrylic copolymer for gold separation from wastewater, Process Saf. Environ. Prot. 106 (2017) 150–162, https://doi.org/10.1016/j.psep.2017.01.002.

[41] Z. Jia, P. Yin, Z. Yang, X. Liu, Y. Xu, W. Sun, H. Cai, Q. Xu, Triphosphonic acid modified multi-walled carbon nanotubes for gold ions adsorption, Phosphorus, Phosphorus Sulfur Silicon Relat Elem. 196 (2020) 106–118, https://doi.org/10.1080/10426507.2020.1818748.

[42] F. Liu, S. Wang, S. Chen, Adsorption behavior of Au(III) and Pd(II) on persimmon tannin functionalized viscose fiber and the mechanism, Int. J. Biol. Macromol. 152 (2020) 1242–1251, https://doi.org/10.1016/j.ijbiomac.2019.10.221.

[43] H.M. Albishri, H.M. Marwani, Chemically modified activated carbon with tris(hydroxymethyl)aminomethane for selective adsorption and determination of gold in water samples, Arab. J. Chem. 9 (2016), https://doi.org/10.1016/j.arabjc.2011.03.017. S252–S258.

[44] G.T. Gebremichael, H. Kim, G.M. Nisola, W.J. Chung, Asparagine anchored on mesoporous silica for Au (III) capture: elucidation of adsorption-reduction mechanisms and their implications towards selective Au (III) recovery, Appl. Surf. Sci. 567 (2021) 150743, https://doi.org/10.1016/j.apsusc.2021.150743.

[45] K. Deng, P. Yin, X. Liu, Q. Tang, R. Qu, Modeling, analysis and optimization of adsorption parameters of Au(III) using low-cost agricultural residuals buckwheat hulls, J. Ind. Eng. Chem. 20 (2014) 2428–2438, https://doi.org/10.1016/j.jiec.2013.10.023.

[46] R.M. Moghazy, A. Labena, S. Husien, E.S. Mansor, A.E. Abdelhamid, Neoteric approach for efficient eco-friendly dye removal and recovery using algal-polymer biosorbent sheets: characterization, factorial design, equilibrium and kinetics, Int. J. Biol. Macromol. 157 (2020) 494–509, https://doi.org/10.1016/j.ijbiomac.2020.04.165.

[47] F. Liu, Z. Zhou, G. Li, Persimmon tannin functionalized polyacrylonitrile fiber for highly efficient and selective recovery of Au(III) from aqueous solution, Chemosphere 264 (2021) 128469, https://doi.org/10.1016/j.chemosphere.2020.128469.

[48] S. Gholamiyan, M. Hamzehloo, A. Farrokhnia, RSM optimized adsorptive removal of erythromycin using magnetic activated carbon : adsorption isotherm , kinetic modeling and thermodynamic studies, Sustain. Chem. Pharm. 17 (2020) 100309, https://doi.org/10.1016/j.scp.2020.100309.

[49] A. Pandiarajan, R. Kamaraj, S. Vasudevan, S. Vasudevan, OPAC (Orange Peel Activated Carbon) derived from waste orange peel for the adsorption of Chlorophenoxyacetic Acid herbicides from water : adsorption isotherm , kinetic modelling and thermodynamic studies, Bioresour. Technol. 261 (2018) 329–341, https://doi.org/10.1016/j.biortech.2018.04.005.

[50] J. Fito, M. Abewaa, A. Mengistu, K. Angassa, A.D. Ambaye, W. Moyo, T. Nkambule, Adsorption of methylene blue from textile industrial wastewater using activated carbon developed from Rumex abyssinicus plant, Sci. Rep. 13 (2023) 5427, https://doi.org/10.1038/s41598-023-32341-w.

[51] N.F.M. Salleh, A.A. Jalil, S. Triwahyono, A. Ripin, S.M. Sidik, N.A.A. Fatah, N. Salamun, N.F. Jaafar, M.H. Hassim, New direct consecutive formation of spinel phase in (Fe,Co,Ni)Al_2O_4 composites for enhanced Pd(II) ions removal, J. Alloys Compd. 727 (2017) 744–756, https://doi.org/10.1016/j.jallcom.2017.08.191.

[52] M.K. Uddin, A. Nasar, Walnut shell powder as a low-cost adsorbent for methylene blue dye: isotherm, kinetics, thermodynamic, desorption and response surface methodology examinations, Sci. Rep. 10 (2020) 1–13, https://doi.org/10.1038/s41598-020-64745-3.

[53] A. Balouch Abdullah, F.N. Talpur, A. Kumar, M.T. Shah, A.M. Mahar, Amina, Synthesis of ultrasonic-assisted lead ion imprinted polymer as a selective sorbent for the removal of Pb^{2+} in a real water sample, Microchem. J. 146 (2019) 1160–1168, https://doi.org/10.1016/j.microc.2019.02.037.

[54] T.H. Bui, W. Lee, S.B. Jeon, K.W. Kim, Y. Lee, Enhanced Gold(III) adsorption using glutaraldehyde-crosslinked chitosan beads: effect of crosslinking degree on adsorption selectivity, capacity, and mechanism, Sep. Purif. Technol. 248 (2020) 116989, https://doi.org/10.1016/j.seppur.2020.116989.

[55] G. Jethave, U. Fegade, S. Attarde, S. Ingle, M. Ghaedi, M.M. Sabzehmeidani, Exploration of the adsorption capability by doping Pb@$ZnFe_2O_4$ nanocomposites (NCs) for decontamination of dye from textile wastewater, Heliyon 5 (2019) e02412, https://doi.org/10.1016/j.heliyon.2019.e02412.

[56] E. Yazdankish, M. Foroughi, M.H.A. Azqhandi, Capture of I^{131} from medical-based wastewater using the highly effective and recyclable adsorbent of g-C3N4 assembled with Mg-Co-Al-layered double hydroxide, J. Hazard Mater. 389 (2020) 122151, https://doi.org/10.1016/j.jhazmat.2020.122151.

[57] S. Dashamiri, M. Ghaedi, A. Asfaram, F. Zare, S. Wang, Multi-response optimization of ultrasound assisted competitive adsorption of dyes onto Cu (OH)2-nanoparticle loaded activated carbon: central composite design, Ultrason. Sonochem. 34 (2017) 343–353, https://doi.org/10.1016/j.ultsonch.2016.06.007.

[58] F. Zandi-Darehgharibi, H. Haddadi, A. Asfaram, Fast and selective adsorption of Au (III) from the waste printed circuit boards using a low-cost adsorbent: optimization by central composite design based on response surface methodology, J. Chem. 2023 (2023), https://doi.org/10.1155/2023/7465722. Article ID 7465722.

[59] D. Xue, T. Li, Y. Liu, Y. Yang, Y. Zhang, J. Cui, D. Ben Guo, Selective adsorption and recovery of precious metal ions from water and metallurgical slag by polymer brush graphene–polyurethane composite, React. Funct. Polym. 136 (2019) 138–152, https://doi.org/10.1016/j.reactfunctpolym.2018.12.026.

[60] L. Liu, S. Liu, Q. Zhang, C. Li, C. Bao, X. Liu, P. Xiao, Adsorption of Au(III), Pd(II), and Pt(IV) from aqueous solution onto graphene oxide, J. Chem. Eng. Data 58 (2013) 209–216, https://doi.org/10.1021/je300551c.

[61] S. Lin, D.H. Kumar Reddy, J.K. Bediako, M.H. Song, W. Wei, J.A. Kim, Y.S. Yun, Effective adsorption of Pd(II), Pt(IV) and Au(III) by Zr(IV)-based metal-organic frameworks from strongly acidic solutions, J. Mater. Chem. A. 5 (2017) 13557–13564, https://doi.org/10.1039/c7ta02518a.

[62] H. Rasoulzadeh, A. Sheikhmohammadi, M. Abtahi, B. Roshan, R. Jokar, Eco-friendly rapid removal of palladium from aqueous solutions using alginate-diatomite magnano composite, J. Environ. Chem. Eng. 9 (2021) 105954, https://doi.org/10.1016/j.jece.2021.105954.

[63] H. Sharififard, M. Soleimani, F.Z. Ashtiani, Evaluation of activated carbon and bio-polymer modified activated carbon performance for palladium and platinum removal, J. Taiwan Inst. Chem. Eng. 43 (2012) 696–703, https://doi.org/10.1016/j.jtice.2012.04.007.

[64] J. Rajahalme, S. Perämäki, A. Väisänen, Separation of palladium and silver from E-waste leachate: effect of nitric acid concentration on adsorption to Thiol scavenger, Chem. Eng. J. Adv. 10 (2022) 100280, https://doi.org/10.1016/j.ceja.2022.100280.

[65] N.R. Biata, S. Jakavula, A. Mpupa, R.M. Moutloali, P.N. Nomngongo, Recovery of palladium and gold from PGM ore and concentrates using ZnAl-layered double Hydroxide@zeolitic imidazolate framework-8 nanocomposite, Separations 9 (2022) 274, https://doi.org/10.3390/separations9100274.

[66] F. Xie, R. Fan, Q. Yi, Z. Fan, Q. Zhang, Z. Luo, Adsorption recovery of Pd(II) from aqueous solutions by persimmon residual based bio-sorbent, Hydrometallurgy 165 (2016) 323–328, https://doi.org/10.1016/j.hydromet.2016.01.005.

[67] E. Cheraghipour, M. Pakshir, Environmentally friendly magnetic chitosan nano-biocomposite for Cu(II) ions adsorption and magnetic nano-fluid hyperthermia: CCD-RSM design, J. Environ. Chem. Eng. 9 (2021) 104883, https://doi.org/10.1016/j.jece.2020.104883.

[68] H. Mazaheri, M. Ghaedi, A. Asfaram, S. Hajati, Performance of CuS nanoparticle loaded on activated carbon in the adsorption of methylene blue and bromophenol blue dyes in binary aqueous solutions: using ultrasound power and optimization by central composite design, J. Mol. Liq. 219 (2016) 667–676, https://doi.org/10.1016/j.molliq.2016.03.050.

[69] R. Khosravi, A. Azizi, R. Ghaedrahmati, V.K. Gupta, S. Agarwal, Adsorption of gold from cyanide leaching solution onto activated carbon originating from coconut shell—optimization, kinetics and equilibrium studies, J. Ind. Eng. Chem. 54 (2017) 464–471, https://doi.org/10.1016/j.jiec.2017.06.036.

[70] T. Şahan, Application of RSM for Pb(II) and Cu(II) adsorption by bentonite enriched with SH groups and a binary system study, J. Water Process Eng. 31 (2019) 100867, https://doi.org/10.1016/j.jwpe.2019.100867.

[71] M. Moghaddari, F. Yousefi, M. Ghaedi, K. Dashtian, A simple approach for the sonochemical loading of Au, Ag and Pd nanoparticle on functionalized MWCNT and subsequent dispersion studies for removal of organic dyes: artificial neural network and response surface methodology studies, Ultrason. Sonochem. 42 (2018) 422–433, https://doi.org/10.1016/j.ultsonch.2017.12.003.

[72] S.J. Mousavi, M. Parvini, M. Ghorbani, Experimental design data for the zinc ions adsorption based on mesoporous modified chitosan using central composite design method, Carbohydr. Polym. 188 (2018) 197–212, https://doi.org/10.1016/j.carbpol.2018.01.105.

[73] V. Mohdee, K. Maneeintr, T. Wannachod, S. Phatanasri, U. Pancharoen, Optimization of process parameters using response surface methodology for Pd(II) extraction with quaternary ammonium salt from chloride medium: kinetic and thermodynamics study, Chem. Pap. 72 (2018) 3129–3139, https://doi.org/10.1007/s11696-018-0542-3.

[74] F. Arshad, M. Selvaraj, J. Zain, F. Banat, M.A. Haija, Polyethylenimine modified graphene oxide hydrogel composite as an efficient adsorbent for heavy metal ions, Sep. Purif. Technol. 209 (2019) 870–880, https://doi.org/10.1016/j.seppur.2018.06.035.

[75] A. Ashrafi, A. Rahbar-Kelishami, H. Shayesteh, Highly efficient simultaneous ultrasonic assisted adsorption of Pb (II) by Fe3O4@MnO2 core-shell magnetic nanoparticles: synthesis and characterization, kinetic, equilibrium, and thermodynamic studies, J. Mol. Struct. 1147 (2017) 40–47, https://doi.org/10.1016/j.molstruc.2017.06.083.

[76] Y. Rakhila, A. Elmchaouri, A. Mestari, S. Korili, M. Abouri, A. Gil, Adsorption recovery of Ag(I) and Au(III) from an electronics industry wastewater on a clay mineral composite, Int. J. Miner. Metall. Mater. 26 (2019) 673–680, https://doi.org/10.1007/s12613-019-1777-x.

[77] H. Javadian, M. Ruiz, A. Maria, Response surface methodology based on central composite design for simultaneous adsorption of rare earth elements using nanoporous calcium alginate/carboxymethyl chitosan microbiocomposite powder containing $Ni_{0.2}Zn_{0.2}Fe_{2.6}O_4$ magnetic nanoparticles: batch and column studies, Int. J. Biol. Macromol. 154 (2020) 937–953, https://doi.org/10.1016/j.ijbiomac.2020.03.131.

[78] M. Jafarnejad, M. Daghighi, F. Afshar, M. Manoochehri, Synthesis of multi-functionalized Fe 3 O 4 -NH 2 -SH nano fi ber based on chitosan for single and simultaneous adsorption of Pb (II) and Ni (II) from aqueous system, Int. J. Biol. Macromol. 148 (2020) 201–217, https://doi.org/10.1016/j.ijbiomac.2020.01.017.

[79] M.R. Neyestani, F. Shemirani, S. Mozaffari, M. Alvand, A magnetized graphene oxide modified with 2-mercaptobenzothiazole as a selective nanosorbent for magnetic solid phase extraction of gold(III), palladium(II) and silver(I), Microchim. Acta 184 (2017) 2871–2879, https://doi.org/10.1007/s00604-017-2299-8.

[80] F.B. Biswas, I.M.M. Rahman, K. Nakakubo, K. Yunoshita, M. Endo, A.S. Mashio, T. Taniguchi, T. Nishimura, K. Maeda, H. Hasegawa, Comparative evaluation of dithiocarbamate-modified cellulose and commercial resins for recovery of precious metals from aqueous matrices, J. Hazard Mater. 418 (2021) 126308, https://doi.org/10.1016/j.jhazmat.2021.126308.